

Ultrafast and low-energy switching in voltage-controlled elliptical pMTJ

Jiefang Deng^{1,2}, Gengchiao Liang^{1,2,}, Gaurav Gupta^{1,3,†}*

¹Department of Electrical and Computer Engineering, National University of Singapore,
Singapore 117576

²Centre for Advanced 2D Materials and Graphene Research Centre, National University of
Singapore, Singapore 117546

³Spin Devices, Delhi 110006, India

Switching magnetization in a perpendicular magnetic tunnel junction (pMTJ) via voltage controlled magnetic anisotropy (VCMA) has shown the potential to markedly reduce the switching energy. However, the requirement of an external magnetic field poses a critical bottleneck for its practical applications. In this work, we propose an elliptical-shaped pMTJ to eliminate the requirement of providing an external field by an additional circuit. We demonstrate that a 10 nm thick in-plane magnetized bias layer (BL) separated by a metallic spacer of 3 nm from the free layer (FL) can be engineered within the MTJ stack to provide the 50 mT bias magnetic field for switching. By conducting macrospin simulation, we find that a fast switching in 0.38 ns with energy consumption as low as 0.3 fJ at a voltage of 1.6 V can be achieved. Furthermore, we study the phase diagram of switching probability, showing that a pulse duration margin of 0.15 ns is obtained and a low-voltage operation (~ 1 V) is favored. Finally, the MTJ scalability is considered, and it is found that scaling-down may not be appealing in terms of both the energy consumption and the switching time for the precession based VCMA switching.

I. INTRODUCTION

Spin transfer torque (STT) based magnetic random access memory (MRAM) [1, 2] because of its non-volatility, high access speed and CMOS (complementary metal oxide semiconductor) compatibility [3] has matured into one of a leading candidate in recent years [4] to fill the memory gap in the extant memory hierarchy. A bit-cell of a STT-RAM comprises of a magnetic tunnel junction (MTJ) which has at least one pinned-layer (PL) and at least one free-layer (FL) with their magnetization in either parallel (P) or anti-parallel (AP) state with respect to (w.r.t.) each other, which corresponds to logic “1” or “0”. In STT-RAM, a free-layer is written by passing a current with density larger than critical current density through the MTJ. If the current is flowing from FL towards PL, a spin-flux with vector parallel to the magnetization of the PL (\mathbf{M}_{PL}) acts on the FL to align the magnetization of the FL (\mathbf{M}_{FL}) with \mathbf{M}_{PL} , whereas if the current direction is reversed a reverse spin-flux with vector anti-parallel to the \mathbf{M}_{PL} acts on the FL to orient it in the AP state. This current based magnetization switching, however, requires a large current density which ranges from 5×10^{10} A-m⁻² for 35 ns to 1×10^{11} A-m⁻² for 2 ns write-time [1, 2] to generate enough spins to toggle all the magnetic moments of the FL. Inevitably, a large current results in considerable Joule heating in the MTJ. This results in self-heating [5-8] induced degradation of the MTJ characteristics, e.g. the spin-polarization of the spin-flux degrades thereby degrading the STT efficiency at the higher temperatures. In addition, electromigration [9, 10] becomes prominent because of the large current densities and the dielectric may also break [11, 12] at the voltages required to sustain the required current densities. Furthermore, to provide a large enough current a bulky access transistor, i.e. with a large channel width-to-length ratio for a bulk-MOSFET or with a large number of fins for a FinFET (Fin Field Effect Transistor), is required. This implies that STT-RAM suffers from high energy consumption, reliability issues and a huge cell area [13, 14].

To reduce the operating current which would subsequently reduce both the energy consumption in the device and the size of the driving transistor, a voltage control of magnetic anisotropy (VCMA) [15] has been promulgated as an alternative to the STT [16, 17]. Since the VCMA based device relies on a voltage rather than a current to write, the current in this case can be greatly reduced by designing a MTJ of a large enough resistance. Furthermore, the VCMA based precessional switching enables the toggling of the FL in sub-ns time regime [15, 18]. Therefore, the energy consumption can be substantially reduced by markedly reducing both the power-dissipation and the dissipation-time. The demonstrations [18-20] hitherto have been on the individual circular pMTJs. These demonstrations require an external in-plane magnetic field to enable the switching. This, however, is not a viable solution for the integrated MRAM w.r.t. both the provision of an external field source and the field uniformity [21, 22]. Consequently, the requirement of an external bias field poses a critical bottleneck for realizing a practical VCMA memory.

In this work, therefore, we propose an elliptical pMTJ to eliminate the requirement of an external magnetic field source. Because of the elliptical structure, via shape anisotropy, an in-plane magnetized bias-layer (BL) separated from the FL by a metallic spacer can be directly engineered within the MTJ stack [23]. This in-plane BL, hence, provides a sufficient bias field for the VCMA based precessional switching. We comprehensively appraise the effects of the electronic, magnetic and physical design constraints on the FL switching dynamics to expound the device physics and an optimal operation window in the proposed design. Our results show that the required bias magnetic field can be contrived within the MTJ stack by an in-plane magnetized BL. For instance, a 10 nm thick BL separated by a 3 nm thick metallic spacer can provide an in-plane exchange field of 50 mT to bias the FL. Furthermore, we show that the FL can toggle in just 0.38 ns consuming only 0.3 fJ at a voltage of 1.6 V across the MTJ, which is attractive for the memory applications. Our results

also indicate that the pMTJ driven by the precession based VCMA favors a low-voltage operation (~ 1 V) with a sufficient margin (0.15 ns) for the applied voltage pulse duration.

This paper is organized as follows. Section II introduces the theoretical method for the simulations. Section III elaborates the operation mechanism for this precession based VCMA switching, followed by the discussion and analysis of different parameters affecting the device properties including a voltage across the MTJ, MgO thickness t_{MgO} , a bias magnetic field and the scalability of the MTJ cross-section. This is followed in Sec. IV by the summary and conclusion of our study.

II. METHODS

Figure 1(a) shows a schematic of an elliptical MTJ with perpendicular magnetic anisotropy (PMA), with major-axis (minor-axis) along x-axis (y-axis). A 1.2 nm thick $\text{Co}_{20}\text{Fe}_{60}\text{B}_{20}$ [24] PL and a 1.7 nm thick $\text{Co}_{20}\text{Fe}_{60}\text{B}_{20}$ FL sandwich a MgO insulator of thickness t_{MgO} . In this work, t_{MgO} ranges from 1.2 nm to 2.8 nm, while the MTJ cross-section ranges from $150 \times 50 \text{ nm}^2$ to $114 \times 38 \text{ nm}^2$ with a fixed aspect-ratio (AR) of 3. Macrospin simulation, which has been shown to be valid in purview of dimensions considered in this work [15, 18, 25, 26], is developed to investigate the magnetization dynamics. The dynamics is described by the Landau-Lifshitz-Gilbert (LLG) equation [27-29] as,

$$\frac{\partial \mathbf{m}}{\partial t} = -\gamma \mathbf{m} \times \mu_0 \mathbf{H}_{\text{Eff}} + \alpha \mathbf{m} \times \frac{\partial \mathbf{m}}{\partial t} + \Gamma_{\text{MTJ_DL}} \mathbf{m} \times \mathbf{p}_{\text{PL}} \times \mathbf{m} + \Gamma_{\text{SV}} \mathbf{m} \times \mathbf{p}_{\text{BL}} \times \mathbf{m} + \Gamma_{\text{MTJ_FL}} \mathbf{m} \times \mathbf{p}_{\text{PL}}, \quad (1)$$

where γ is the gyromagnetic ratio, μ_0 is the vacuum permeability, $\alpha = 0.01$ [28] is the Gilbert damping coefficient for $\text{Co}_{20}\text{Fe}_{60}\text{B}_{20}$, and \mathbf{p}_{PL} (\mathbf{p}_{BL}) is a unit-vector anti-parallel (parallel) to the magnetization of the PL (BL). The magnetization unit-vector of the FL \mathbf{m} is $[m_x \ m_y \ m_z]$, which is $[0 \ 0 \ \pm 1]$ in stable states, with m_x , m_y and m_z being the projections on the respective axis denoted by the subscripts. \mathbf{H}_{Eff} is the effective magnetic field experienced by the FL. It is

the vector sum of a uniaxial anisotropy field \mathbf{H}_K , a demagnetizing field \mathbf{H}_D , a thermal fluctuation field $\mathbf{H}_{\text{Therm}}$, and an external bias field \mathbf{H}_{Bias} , which are expressed as,

$$\mathbf{H}_K = \frac{2 K_U}{\mu_0 M_S} [0, 0, m_z], \quad K_U = K_{U_Bulk} + \frac{K_{I0} - \xi \cdot E_z}{t_{FL}}, \quad (2)$$

$$\mathbf{H}_D = -M_S [N_x m_x, N_y m_y, N_z m_z], \quad (3)$$

$$\mathbf{H}_{\text{Therm}} = \sqrt{\frac{2 \alpha K_B T}{(1 + \alpha^2) \gamma M_S V(\Delta t)}} \frac{1}{\mu_0} [G_{(0,1)}^x, G_{(0,1)}^y, G_{(0,1)}^z], \quad (4)$$

where K_U is the anisotropy energy density with contributions from the bulk anisotropy, K_{U_Bulk} , and the interfacial anisotropy K_I . The latter is computed as $K_{I0} - \xi \cdot E_z$. As implied from eq. (2), the interfacial anisotropy is assumed to be linearly modified by the perpendicular component E_z of the electric-field \mathbf{E} at the MgO-FL interface, at a rate determined by the VCMA coefficient ξ [24, 30], where eq. (2) assumes a positive value of E_z for the field direction shown in Fig. 1(a). For the voltage applied across the MTJ V_{MTJ} , the magnitude of E_z is assumed to be $V_{\text{MTJ}}/t_{\text{MgO}}$, assuming an entire potential drop across the insulator [18, 20]. The CoFeB and the CoFeB/MgO interface parameters like saturated magnetization $M_S = 1.257 \times 10^6 \text{ A}\cdot\text{m}^{-1}$, $K_{U_Bulk} = 2.245 \times 10^5 \text{ J}\cdot\text{m}^{-3}$, $K_{I0} = 1.286 \times 10^{-3} \text{ J}\cdot\text{m}^{-2}$ [24] and $\xi = 50 \text{ fJ}\cdot\text{V}^{-1}\cdot\text{m}^{-1}$ [31] are the empirical parameters from the experimental papers. The value of ξ at the CoFeB/MgO interface in literature is in the range of 20-100 $\text{fJ}\cdot\text{V}^{-1}\cdot\text{m}^{-1}$ [31-34]. More efficient VCMA effect, i.e. a large ξ , would result in even better performance of the proposed device than that predicted in this work.

In eq. (3), N_x , N_y and N_z are the demagnetizing factors along x, y and z direction, which are determined by the shape and the size of the magnet (shape anisotropy) [35, 36]. The dipole field from the PL has been neglected assuming that this dipole field can be cancelled out by synthetic ferrimagnetic reference layers [37]. Thermal fluctuation is described by eq. (4), where K_B , V and Δt are the Boltzmann constant, the FL volume and the calculation time

step of 5 ps, respectively. The stochastic partial differential equation (SPDE) described by eq. (1) is integrated via fourth order Runge-Kutta method [38-40]. An alternate method for solving this SPDE is first-order Euler method [41, 42], and the trade-offs between the methods are discussed in Refs. [38, 43] for a more interested reader. The device is assumed to operate at the room temperature ($T = 300$ K), and the self-heating effects due to Joule heating have been ignored because the VCMA devices, including the one discussed in this work with data shown in the next section, operate at much lower current densities than the traditional STT devices. $G_{(0,1)}$ with superscript along the respective axis are the independent random numbers computed at every time-step and each has a Gaussian distribution with zero mean and unit standard deviation [44]. \mathbf{H}_{Bias} (c.f. Fig. 1(a)) is provided by an in-plane magnetized BL (Co/Pt multilayers) via its dipole field, which is calculated by micromagnetics simulation using MuMax3 simulator [45]. The simulation cell size is chosen to be 1 nm along all three dimensions. Since \mathbf{H}_{Bias} is only along the x-axis in this study, subsequently, it is represented by a scalar quantity H_x . The damping-like torque (DLT) with a linear dependence on V_{MTJ} , and the field-like torque (FLT) with a quadratic dependence on V_{MTJ} are respectively obtained as,

$$\Gamma_{\text{MTJ_DLT(SV)}} = \frac{\hbar}{2e} \frac{\gamma \eta_{\text{MTJ(SV)}}}{V R_{\text{MTJ}}} V_{\text{MTJ}}, \quad \Gamma_{\text{MTJ_FLT}} = v \frac{\hbar}{2e} \frac{\gamma \eta_{\text{MTJ}}}{V R_{\text{MTJ}}} V_{\text{MTJ}}^2, \quad (5)$$

where \hbar is the reduced Planck constant, e is the charge of an electron, R_{MTJ} is the resistance of the MTJ, $\eta_{\text{MTJ(SV)}}$ is the STT efficiency, and $v = 2.97/7.82 \text{ V}^{-1}$ is the ratio between the two torques extracted from Ref. [46] (see Table 2.1 and 2.2 of thesis from Kerstin Bernert [47] for the range of values in literature). Analysis of R_{MTJ} includes the voltage dependence of the tunneling magnetoresistance (TMR) and the dynamic angle θ between the FL and PL as,

$$R_{\text{MTJ}} = R_{\text{P}} + \frac{R_{\text{APO}} - R_{\text{P}}}{1 + \frac{V_{\text{MTJ}}^2}{V_{\text{Half}}^2}} \left(\frac{1 - \cos(\theta)}{2} \right), \quad (6)$$

where $V_{\text{Half}} = 0.4$ V, extracted for CoFeB from Ref. [20, 48], is the voltage across a MTJ at which TMR becomes half of its value at zero-bias i.e. $\text{TMR}_0/2$. R_P is the MTJ resistance when both magnets are exactly parallel (P) to each other and assumed to remain invariant to V_{MTJ} for all practical purpose [46, 49], while $R_{\text{AP}0}$ is the MTJ resistance when both magnets are exactly anti-parallel (AP) to each other at a zero-bias. Since in the recent years Slonczewski expression [27] for spin-torque efficiency has been extended to account for multiple reflections of the spin-flux in the spin valves [50-53], the STT effect by the BL in this study is based on the multi-reflection model. Hence, the STT efficiencies for the PL-MgO-FL MTJ (η_{MTJ}) and the FL-Metal-BL spin valve (η_{SV}) are computed as [52, 54],

$$\eta_{\text{MTJ}} = \frac{P_1 / 2}{1 + P_1^2 \cos(\theta)}, \text{ where } P_1 = \sqrt{\frac{\text{TMR}_0 / 2}{1 + \text{TMR}_0 / 2}}, \quad (7)$$

$$\eta_{\text{SV}} = \frac{P_2 - P_2 \zeta \cos(\theta)}{1 - \zeta^2 \cos^2(\theta)}, \text{ where } \zeta = 1 - 2\varepsilon + 2\varepsilon^2 \text{ and } \varepsilon = \frac{1 - P_2}{2}, \quad (8)$$

where P_1 is obtained from Julliere's formula for equal polarization of FL and PL [55] and $P_2 = 0.35$ [56].

III. RESULTS

A. Operation Principle

Since in a VCMA based MTJ, the interfacial anisotropy energy can be tuned by an applied voltage, the competition between the uniaxial anisotropy and the demagnetizing field, which determines the easy axis direction, can be controlled by the voltage. Specifically, considering the bulk and the interface PMA with the demagnetization simultaneously, the net anisotropy energy density becomes,

$$K_{\text{U_Eff}} = K_{\text{U}} - \frac{1}{2} \mu_0 M_{\text{S}}^2 N_{\text{Z}}. \quad (8)$$

When $K_{U_Eff} > 0$, FL has a perpendicular magnetization i.e. it has the easy-axis along the z-axis. If $K_{U_Eff} < 0$, the magnet has the easy-axis along the major-axis of the elliptical FL i.e. the x-axis in this work. Among the parameters in eq. (2) and (8), t_{FL} and N_Z depend on the physical dimensions of the magnet and remain fixed once the MTJ is fabricated in accordance with the design specifications, while E_Z can be dynamically modified by controlling V_{MTJ} . For the precession based VCMA switching of the pMTJ devices [18, 20], these physical and electrical controls are designed such that in the absence of a V_{MTJ} , K_U which equals $K_{U_Bulk} + K_{I0}/t_{FL}$ is large enough for K_{U_Eff} to be positive. However, the V_{MTJ} is designed to be large enough to have a sufficient E_Z that can render K_{U_Eff} to a computationally negative value. Physically, this implies that the FL destabilizes along the z-axis and its easy-axis now aligns along the x-axis, thereby forcing \mathbf{m} of the FL to tend towards a new stable state governed by the \mathbf{H}_{Eff} and the STT. Conversely, if a negative voltage pulse is applied, as evident from eq. (2) and (8), K_{U_Eff} becomes more strongly positive because the interface anisotropy is enhanced. Categorically, this has been suggested as a scheme to read MTJ with an increased reliability [57]. The critical values, at which K_{U_Eff} is zero and thus the orientation of the easy-axis changes, are defined as follows in this study. The critical thickness of FL, in the absence of E_Z , is symbolized by t_{FLC} , while V_C and E_{ZC} , respectively, symbolize the critical values of V_{MTJ} and E_Z for a given t_{FL} . Furthermore, the applied V_{MTJ} should not exceed the dielectric breakdown field E_{Break} for MgO insulator [11] which is slightly over 2 V-nm^{-1} . Hence, the device is designed such that in absence of a V_{MTJ} , K_{U_Eff} is positive, while it becomes negative for a V_{MTJ} pulse (c.f. Fig. 1(b)) where $E_{ZC} < V_0/t_{MgO} < E_{Break}$. The design is furthermore constrained by a maximum permissible voltage in the system which is not discussed in this study because it is subjective to the targeted application and the desired stability factor Δ of the FL. Δ is computed *in the absence of* V_{MTJ} and described as [58],

$$\Delta = \Delta_0 \left(1 - \frac{H_x}{H_K^{\text{Eff}}} \right)^2, \text{ where } \Delta_0 = \frac{K_{U_Eff}}{K_B} \frac{V}{T} \text{ and } H_K^{\text{Eff}} = \frac{2 K_{U_Eff}}{\mu_0 M_s}. \quad (9)$$

If the FL is permanently biased as in this work, the stability can be reduced quadratically as a result of the bias field, whereas if H_x is applied only during the write operation [59], Δ can be substantially increased to equal Δ_0 . The scheme suggested in Ref. [59] depends on the Oersted field generated around the current carrying wire in the adjacent cells. Consequently, for a substantial H_x firstly it becomes power intensive and secondly this acts as a stray field and disturbs other bit-cells thereby limiting the memory density. Therefore, an alternative scheme of increasing Δ without compromising with V_{MTJ} or reducing H_x would be an important future direction.

For a precession based VCMA switching of the pMTJ devices, a V_{MTJ} as a trapezoidal pulse of duration t_{Pulse} is applied to toggle the FL, as shown in Fig. 1(b). A finite rise and fall time, t_{Rise} and t_{Fall} , respectively, of 50 ps is assumed to consider a non-ideal input. A full-scale voltage V_0 , which exceeds V_C , is applied for time t_{High} duration to temporarily change the easy-axis from z - to x -axis. A non-zero pulse is then applied for duration $t_{\text{ON}} = t_{\text{Rise}} + t_{\text{High}} + t_{\text{Fall}}$. This induces the precession of \mathbf{m} around the shifted \mathbf{H}_{Eff} . A sufficiently large H_x allows the FL m_z to swing from +1 to -1 and vice versa as illustrated in Fig. 2 (a-c) for the FL of thickness t_{FL} 1.7 nm, cross-section $150 \times 50 \text{ nm}^2$, t_{MgO} of 2 nm, V_0 of 1.6 V and $\mu_0 H_x$ of 50 mT. As shown in Fig. 2 (a-c), by designing t_{ON} to be odd or even multiples of the half-precession period ($t_{\text{Half}} = 0.35 \text{ ns}$ for the shown cases), the m_z toggles or comes back to the original state, respectively. A long enough time of t_{OFF} ensures that the \mathbf{m} relaxes to the z -axis. Consequently, the final state of \mathbf{m} strongly depends on t_{ON} since it determines if \mathbf{m} is above or below the x - y plane when the V_{MTJ} goes to zero and the easy-axis is switched back along the z -axis. This implies that pulse duration should be controlled in a certain range to have a deterministic switching. Notably, if t_{High} is comparable with or larger than the relaxation time

so that \mathbf{m} would damp to align and lock with the \mathbf{H}_{Eff} or if the rise and fall time are comparable with or larger than t_{Half} , the switching would become extremely sensitive to the transition times i.e. t_{Rise} and/or t_{Fall} . The study of the effect of t_{Rise} and t_{Fall} is, however, not considered in the current work because a voltage pulse with 50 ps rise/fall time can be generated with a jitter at sub 10 picosecond to femtosecond scale [60, 61], which in fact is at least two orders smaller than the t_{Half} . The effect of t_{Rise} and t_{Fall} is thus assumed to be negligible compared with other parameters in this study.

Pessimistically, the deterministic switching based on the precise control of the precession cycles requires a bias magnetic field. As mentioned in eq. (1), the \mathbf{H}_{Eff} experienced by the FL includes \mathbf{H}_{K} , \mathbf{H}_{D} and $\mathbf{H}_{\text{Therm}}$. Among them, the \mathbf{H}_{K} only has a z-component field while the \mathbf{H}_{D} and the $\mathbf{H}_{\text{Therm}}$ can be non-zero along the x-axis. However, the small N_x due to the FL dimensions in eq. (3) and the thermal fluctuation as a perturbation are unable to provide a large enough x-component field to support a full-scale precession around the x-axis. As a result, the application of a bias field H_x is seemingly indispensable. To simplify the design for generating the H_x , an elliptical pMTJ is used, which allows an in-plane magnetized BL separated by a metal spacer to be fabricated within the MTJ stack (c.f. Fig. 1(a)). The dipole field provided by the BL is shown in Fig. 2(d). It shows that, typically as expected, a thinner metal spacer results in a stronger bias field because a dipole field strengthens as the distance from the magnet decreases. Intuitively, thickening the BL, while ensuring that a single domain is maintained, would have more magnetic moments along the x-axis, which then would lead to a larger bias field for the same t_{M} . Hence, the t_{M} and the t_{BL} can be custom designed to obtain the required H_x . In this work, the $\mu_0 H_x$ applied on the MTJ is approximately 50 mT. As shown in Fig. 2 (d), this large H_x can be provided via a 10 nm thick BL with the metal spacer of t_{M} 3 nm, implying that an elliptical MTJ stack can function without an additional external system to provide the bias field.

Furthermore, in Fig. 2, the t_{MgO} is thick enough (2 nm) for the chosen V_0 to render the STT ineffective. In case the MgO is thin and/or V_0 is large enough so that the STT is strong, STT would also play an important role in the FL dynamics as evident from eq. (1). For the configuration in Fig. 1(a), the electrons flow from FL to PL and thus a reflected spin-flux oriented anti-parallel to \mathbf{M}_{PL} acts on the FL, i.e. along the $-z$ -axis in this case and thus STT effect attempts to damp \mathbf{m} towards the $-z$ -axis. This has following important implications on the switching. Pure VCMA effect would be symmetric w.r.t. switching from P-to-AP or vice versa state of the MTJ, but the STT would introduce an asymmetry in the dynamics. Since, $[0 \ 0 \ -1]$ spins act on the FL, it becomes easier (faster, reliable and more energy efficient) to toggle into or retain $m_z = -1$ state, but it becomes difficult to toggle into or retain $m_z = +1$ state. Therefore, if the PL had been pinned along the z -axis then for the MTJ in presence of a non-negligible STT effect, switching into an AP state would be easier than into a P state.

B. V_{MTJ} Dependence

First we investigate the electronic control of the device which allows designer to easily and dynamically tune the performance post-fabrication of the device. To probe the effects of V_0 on the precession based VCMA switching in an elliptical pMTJ, a representative FL of size $150 \times 50 \times 1.7 \text{ nm}^3$ is chosen. A t_{MgO} of 2 nm, resistance-area (RA) product of $1820 \ \Omega\text{-}\mu\text{m}^2$, and a zero voltage-bias tunnel magnetoresistance ratio (TMR_0) of 144% is picked from Ref. [20]. A 50 mT bias field along x -axis H_x is applied to assist the switching. This in-plane field, however, reduces the FL thermal stability from 138 to 28 as calculated from eq. (9). This greatly shrunk thermal stability limits the applicability of the proposed elliptical pMTJ in the storage class memories (SCMs) [62, 63] and the enterprise storage [64] which need a retention time on the scale of months to 10 years or more [63-66]. However, because of the ultra-low power sub-ns writing in this design, and the stability which suffices the requirements for an

embedded non-volatile cache memory [57, 67, 68], the promulgated precessional VCMA based MRAM may be a promising replacement for a power-intensive volatile static random-access memory (SRAM) in the cache. The detailed appraisal of the performance metrics for a VCMA based MRAM [57] is beyond the purview of our current work and we focus on the device physics of the proposal. Furthermore, this stability also suffices for the MTJ based non-volatile logic (NVL) [69].

The phase diagrams of the switching probability for switching from P-to-AP (P10) and from AP-to-P (P01) are shown in Fig. 3(a) and (b), respectively. For sweeping t_{ON} , t_{High} is swept while t_{Rise} and t_{Fall} are held constant at 50 ps each. Each colour point is determined by simulating the device 100 times under the identical conditions while considering thermal fluctuation. Red regions (operation windows), which are directly related to the precession period, signify a deterministic toggling, i.e. 100% probability of switching, while the dark-blue regions denote an unaltered \mathbf{m} state i.e. 100% probability that the original magnetic-state is retained. For a given V_0 , the probability oscillates between 0 (the dark-blue regions) and 1 (the red regions) with t_{ON} because for the odd and even multiples of t_{Half} , the FL toggles and gets restored to the original state, respectively. However, at small V_0 and large t_{ON} , the switching is nondeterministic and probability is approximately 50%, as also observed experimentally in Ref. [15]. This is because at low V_0 and large t_{ON} , the VCMA effect is relatively weak and the t_{High} is comparable with the relaxation time, thus failing to keep the precession about the x-axis for a long time and resulting in an uncertain final state in the presence of the thermal fluctuation. Comparing Fig. 3(a) with 3(b) shows that there is no significant difference in the phase diagram for P10 and P01, which implies that there is symmetry in the switching from P-to-AP and AP-to-P state, indicating that the STT effect is negligible. Next, the black curve with the bars indicates deterministic switching without thermal fluctuation to explicitly illustrate the effect of the thermal fluctuations for the fastest t_{ON} scenario. This t_{ON} is chosen to

equal t_{Half} . As shown in Fig. 3(a) and (b), the operation window shrinks, as expected, when the thermal fluctuation is considered, implying that for a precession based VCMA switching the thermal fluctuation perturbs the deterministic toggling. Moreover, the operation window expands as the V_0 diminishes. This is because the reduced V_0 weakens the VCMA effect, resulting in a stronger interfacial anisotropy field along the z-axis as evident from eq. (2). This tends to increase the magnitude of m_z and reduce m_x thus subduing shape anisotropy field along the x-axis, resulting in the reduction of the x-component of \mathbf{H}_{Eff} . The \mathbf{m} still precesses around the x-axis, although its trajectory is now not totally symmetrical about the x-y plane. Because the precessional period is inversely proportional to the magnetic field along the precession-axis, which is nearly along the x-axis, with a reduced field along the x-axis the precessional period increases. As a result, the operation window, which is closely related to the precession period, increases as V_0 decreases. A larger operation window implies more tolerance in variation for t_{High} , and hence, a more reliable write-operation, indicating that the low-voltage operation is achievable for this studied device.

The V_0 dependence of the current density J through the MTJ and the energy consumption E is shown in Fig. 3(c) and (d), respectively, for both P-to-AP and AP-to-P switching for a unit probability with t_{ON} equal to a respective t_{Half} . Because the J is changing during the switching process, values are extracted when the V_{MTJ} first reaches V_0 (see Fig. 1(b)). Consequently, the J from P-to-AP is slightly larger than that from AP-to-P because of a different initial MTJ resistance. In addition, as expected, the J increases linearly as the V_0 increases, and remains in the order of 10^8 A-m⁻² because of a thick enough (2 nm) MgO layer. This low current density then ensures a relatively low switching energy as seen in Fig. 3(d). The switching energy has two components,

$$E = \int_0^{t_{\text{ON}}} \frac{(V_{\text{MTJ}}(t))^2}{R_{\text{MTJ}}(t)} dt + \frac{1}{2} \frac{\epsilon_0 \epsilon_{\text{MgO}} A}{t_{\text{MgO}}} V_0^2, \quad (10)$$

where $\epsilon_{\text{MgO}} = 9.7$ [70] is the relative permittivity of MgO, ϵ_0 is the vacuum permittivity, and A is the cross-sectional area of the MTJ. The first term in eq. (10) is the Joule heating E_J , and second term is the charging energy E_C consumed by the MTJ capacitance. The capacitance has been assumed to be independent of the relative magnetization of PL and FL because of the sub- μm^2 cross-section of the MTJ [71]. E_C ranges from 0.046 fJ to 1.138 fJ for V_0 from 0.6 V to 3 V, which is 9% to 14% of E (0.5 fJ to 8.1 fJ), respectively. Because of a large MTJ resistance at t_{MgO} of 2 nm, the current density stays lower than $2 \times 10^9 \text{ A}\cdot\text{m}^{-2}$, and a low switching energy ($<10 \text{ fJ/switch}$) is achieved (c.f. Table I of Ref. [69] for a general comparison with other non-volatile memory technologies). Moreover, Fig. 3(e) exhibits the switching probability from P-to-AP ‘AND’ AP-to-P as a function of t_{ON} and V_0 . Red regions denote a deterministic switching, i.e. 100% certainty of toggling. At $V_0 = 1 \text{ V}$, the corresponding operation window of t_{ON} is from 0.31 ns to 0.46 ns i.e. 0.15 ns, a decent margin for t_{High} to vary without affecting the reliable operation. On the other hand, Fig. 3(f) presents the retention probability as a function of t_{ON} and V_0 . Red regions show with 100% probability that pre-configured data is not disturbed. As a consequence, the red regions can be used for reading, e.g. as long as the read voltage is below 0.4 V, the FL magnetic state will always remain unaltered, which implies that an absolutely disturb-free read operation can be achieved for the MRAM application.

C. MgO Thickness Dependence

As demonstrated in the previous section, the device prefers a low-voltage operation for a decent pulse duration margin unto a value at which further decreasing V_0 may fail the switching. Hence, to study the t_{MgO} dependence on the switching, V_0 is fixed to be 1.6 V in this section. This V_0 allows a sufficient t_{MgO} variation range to achieve low energy consumption as expounded later. RA-products, TMRs and V_{Half} for a different MgO

thicknesses are extracted from the experimental paper [20]. For a fixed V_0 as the t_{MgO} decreases, principally, both VCMA and STT effect become stronger. The former becomes stronger because the E_z at the MgO-FL interface becomes stronger (see eq. (2)). Simultaneously, the RA-product decreases exponentially as the t_{MgO} decreases. Since the current density J is inversely proportional to the RA-product, J thus increases exponentially from $10^7 \text{ A}\cdot\text{m}^{-2}$ to $10^{10} \text{ A}\cdot\text{m}^{-2}$ for a decreasing t_{MgO} , as shown in Fig. 4(a), which makes the STT increasingly stronger. Next, the t_{ON} in Fig. 4(b), which is chosen to equal t_{Half} , shows an increasing trend as t_{MgO} increases because of a vitiating VCMA effect. At large t_{MgO} , the two curves overlap and a linear relation is observed. The linear relation is observed on account of the fact that t_{ON} is inversely proportional to the precession frequency which in turn is almost proportional to \mathbf{H}_{Eff} . The \mathbf{H}_{Eff} varies linearly with $\mathbf{H}_{\mathbf{K}}$, and $\mathbf{H}_{\mathbf{K}}$ is inversely proportional to t_{MgO} (see eq. (2)) because of the VCMA effect. This indicates that the VCMA effect dominates over the STT effect for large t_{MgO} . For small t_{MgO} , there is a divergence in t_{ON} between P-to-AP (black solid circles) and AP-to-P (red triangles) switching trends, implying that the STT effect is substantial which can be understood as follows. Beyond the critical electric field which changes the easy axis from z- to x-axis, further strengthening of the VCMA effect is inessential and has no significant additional contribution in the switching. However, STT effect has no such upper threshold in this case and starts to dictate the switching dynamics. For P-to-AP switching, since the electron flow direction is from FL to PL and due to the STT effect, the FL receives spin-flux anti-parallel to the magnetization of the PL. As a result, the STT effect assists the VCMA effect to attain an AP state for the FL and accelerates the switching process. In contrast, for AP-to-P switching, the STT effect contests with the VCMA effect to switch the FL. The FL still receives the spin-flux anti-parallel to the PL magnetization due to the STT effect and hence endeavors to maintain the FL in the AP-state. Conversely the VCMA effect strives to toggle the FL into a P-state. The two effects thus jostle

to toggle the FL. This decelerates the toggling, which results in a larger t_{ON} for the AP-to-P case. Moreover, because of the increasingly stronger dominance of the STT effect, the slope for the P-to-AP switching trend line increases as the t_{MgO} decreases. However, for AP-to-P switching, on reducing the t_{MgO} , the t_{ON} slope tends to transit from positive to negative.

As discussed in the previous section, the charging energy E_C is a fraction of the Joule heating. When the STT effect is substantial, the net energy consumed (E) trend shown in Fig. 4(c) nearly follows the declining trend of the current density shown in Fig. 4(a). Nevertheless, when the t_{MgO} becomes thicker than 2.2 nm, E_C becomes comparable to E_J because of the exponential decline in the current density and the corresponding Joule heating. Figure 4(c) also shows that as the STT effect wanes-off and VCMA dominates for a large t_{MgO} , the slope of E tapers down and E finally approaches 0.3 fJ, which is also the minimum energy achieved in this work. Figure 4(d) and (e), respectively, show the phase diagrams of the switching probability from P-to-AP (P10) and from AP-to-P (P01) as a function of t_{ON} and t_{MgO} . An obvious oscillatory dependence on t_{ON} is observed. At a large t_{MgO} and for long pulse duration, the oscillations disappear because of the weak VCMA effect. Interestingly in Fig. 4(d), there is a sharp decrease in the t_{ON} operation window for the first half precession cycle for a small t_{MgO} (the red region on the left-bottom around $t_{MgO} = 1.6$ nm). This happens because in the said region a strong STT effect compliments the VCMA effect for P-to-AP switching, and greatly accelerates the switching process. This sharply reduces the precession period and the scope for tolerating variations in t_{High} . For a larger t_{MgO} , a wider operation window indicates that the device can tolerate more variations in t_{High} in this regime. It can be found that it is more favorable to design the device with a large MgO thickness in the purview of a critical VCMA field for a given V_0 , because both a larger margin in the pulse variation for the deterministic switching and a lower write-energy can be achieved in this regime.

D. MTJ Scalability and Bias Magnetic Field

As noted earlier, the external bias field required in the precession based VCMA switching has been a critical bottleneck in advancing it for memory applications and therefore in this work, the elliptical pMTJs have been presented so that H_x can be engineered within the stack and provided by a BL. Besides the thickness of the BL discussed earlier, it is the cross-section of the MTJ which determines the number of magnetic moments in the BL for providing the bias-field through the FL that is to be toggled. Furthermore, the demagnetizing field scales with the cross-section thereby modifying the switching-time, required bias-field and energy landscape. Therefore, the MTJ cross-section is an important physical constraint to investigate to comprehend the device physics in the proposed VCMA device.

The effect of H_x on the switching probability is shown in Fig. 5(a) and (b). For a pMTJ with FL of $150 \times 50 \times 1.7 \text{ nm}^3$ dimensions, t_{MgO} of 2 nm and V_0 of 1.6 V, there is a limited functional region in the range of 38-58 mT for $\mu_0 H_x$. This range can be shifted for different conditions. As seen from Fig. 5(a) and (b), increasing the bias field H_x shrinks the red region, i.e. the operation window, which is similar to the case exhibited in Fig. 3(a) and (b). When the $\mu_0 H_x$ increases to more than 58 mT, an excessively strong \mathbf{H}_{Eff} results in an overly fastened precession, thus sharply reducing the relaxation time, which is too fast to allow a deterministic switching. Conversely, if the $\mu_0 H_x$ is insufficient, i.e. less than 38 mT, a deterministic switching around the x-axis would not be supported. Hence, a probabilistic final state is attained by virtue of the thermal fluctuation. Approximately 50% switching probability is also observed when the pulse duration lasts long enough for a smaller $\mu_0 H_x$. This is because the large t_{ON} provides enough time for the magnetization to relax along the x-axis. Once the voltage is removed, the easy-axis switches back to the z-axis, thus \mathbf{m} would relax to either +z or -z-axis depending on the thermal fluctuation with equal probability. To reduce the required H_x for switching, one possible way is to design the FL thickness even

closer to the critical thickness but this would further sacrifice the thermal stability for instance for the NVL applications. This adjustment has three effects: it would weaken both the interfacial anisotropy and the demagnetizing field along the z-axis, and enhance the demagnetizing field along the x-axis. All of these would enable the operation at smaller V_C . In consequence, a stronger VCMA effect is obtained at the same V_0 , which then relieves the requirement for a larger $\mu_0 H_x$.

Scalability of the pMTJ is next investigated in Fig. 5(c) and 5(d). The AR is held at 3, FL thickness at 1.7 nm, t_{MgO} at 1.5 nm and V_0 at 1.6 V, while the length and width of the MTJ is swept. The bars in Fig. 5(c) represent the operation windows, which are extracted by simulating the devices 100 times under identical conditions (thermal fluctuations enabled). Within the operation window, switching happens with 100% certainty. Figure 5(c) shows that when the MTJ cross-section (represented as MTJ width) is scaled down, the optimal t_{ON} (the data-markers on the curve), which equals respective t_{Half} , increases. This happens because on scaling down the MTJ, the N_z decreases which thus increases the $K_{\text{U_Eff}}$. As a result, the critical voltage V_C (c.f. the inset), where $K_{\text{U_Eff}} = 0$, as seen from eq. (2) and (8), becomes larger. In consequence, it is more difficult to switch. Hence, it takes larger t_{ON} or the switching may even fail altogether. In addition, a considerable operation window is achieved for the MTJ cross-section between $39 \times 117 \text{ nm}^2$ and $45 \times 135 \text{ nm}^2$. On scaling down the MTJ cross-section below $39 \times 117 \text{ nm}^2$, the deterministic switching fails because the switching becomes increasingly implausible, unless V_0 or H_x is increased as discussed earlier. On the other hand, for the MTJ cross-section above $\sim 45 \times 135 \text{ nm}^2$, the operation window narrows as a result of the fastened precession process.

For the designs in Fig. 5(c), the respective energy consumption is shown in Fig. 5(d). At first a descending and then an ascending trend is observed. This behaviour is due to the competition between the t_{ON} and the MTJ resistance as evinced in eq. (10). The former

increases as observed in Fig. 5(c), while the latter also increases because for a given RA-product, the MTJ resistance increases as the MTJ cross-section is scaled down. These two have opposite contributions to the Joule heating; therefore, the trends exhibit a local minima where both t_{ON} and MTJ resistance are optimized to deliver the lowest energy switching. These trends also imply that unduly scaling down the MTJ cross-section may not be attractive in terms of the energy consumption.

IV. CONCLUSION

We propose and appraise the elliptical pMTJs for a voltage controlled precessional switching. The V_{MTJ} , t_{MgO} , STT, bias magnetic field and MTJ scalability effects on the pMTJ properties are investigated. We show that an in-plane magnetized BL designed within the MTJ stack can bias the FL to eliminate the need of providing a uniform in-plane magnetic field for the FL by additional equipment or an external circuit. The pMTJ can be switched for as low as 0.3 fJ in just 0.38 ns at 1.6 V. Furthermore, it is shown that the Joule heating can be adequately suppressed by increasing t_{MgO} . We also find that the design favors to operate at low voltage (~ 1 V) and large MgO thickness. There is also a sufficient margin for the variation in t_{High} without affecting the reliable operation. This should be encouraging for a practical disposition of the VCMA based MRAM. The advantages like fast switching, ultra-low energy consumption and non-volatility are very attractive for VCMA based MRAM application in the cache memories.

Corresponding Authors

*elelg@nus.edu.sg †gauravdce07@gmail.com

ACKNOWLEDGEMENTS

This work at the National University of Singapore was supported by CRP award no. NRF-CRP12-2013-01 and MOE2013-T2-2-125. We gratefully acknowledge the discussions with Xuanyao Fong, and the funding support from the National Research Foundation, Prime Minister Office, Singapore, under its Medium Sized Centre Programme.

References

- [1] A. Khvalkovskiy, D. Apalkov, S. Watts, R. Chepulskii, R. Beach, A. Ong, X. Tang, A. Driskill-Smith, W. Butler and P. Visscher, Basic principles of STT-MRAM cell operation in memory arrays, *J. Phys. D: Appl. Phys.* 46, 074001 (2013).
- [2] D. Apalkov, B. Dieny and J.M. Slaughter, Magnetoresistive Random Access Memory, *Proc. IEEE* 104, 1796-1830 (2016).
- [3] M.C. Gaidis, *Magnetic Back-End Technology, Introduction to Magnetic Random-Access Memory*, John Wiley & Sons, Inc., 165-198 (2017).
- [4] Y. Nishi, *Advances in Non-volatile Memory and Storage Technology* (Woodhead Publishing, Cambridge, 2014).
- [5] C. Chul-Min, O. Young-Taek, K. Kyung-Jun, P. Jin-Suk, S. Hiroaki, M. Seiji, K. Sung-Kyu, L. Jeong-Yong and S. Yun-Heub, Temperature dependence of reliability characteristics for magnetic tunnel junctions with a thin MgO dielectric film, *Semicond. Sci. Technol.* 31, 075004 (2016).
- [6] B. Oliver, G. Tuttle, Q. He, X. Tang and J. Nowak, Two breakdown mechanisms in ultrathin alumina barrier magnetic tunnel junctions, *J. Appl. Phys.* 95, 1315-1322 (2004).
- [7] K. Hosotani, M. Nagamine, T. Ueda, H. Aikawa, S. Ikegawa, Y. Asao, H. Yoda and A. Nitayama, Effect of self-heating on time-dependent dielectric breakdown in ultrathin MgO magnetic tunnel junctions for spin torque transfer switching magnetic random access memory, *Jpn. J. Appl. Phys.* 49, 04DD15 (2010).
- [8] C.-M. Choi, Y.-T. Oh, K.-J. Kim, J.-S. Park, H. Sukegawa, S. Mitani, S.-K. Kim, J.-Y. Lee and Y.-H. Song, Temperature dependency of reliability characteristics for magnetic tunnel junctions with a thin MgO dielectric film, *Semicond. Sci. Technol.* 31, 075004 (2016).
- [9] J. Ventura, J.B. Sousa, Y. Liu, Z. Zhang and P.P. Freitas, Electromigration in thin tunnel junctions with ferromagnetic/nonmagnetic electrodes: Nanoconstrictions, local heating, and direct and wind forces, *Phys. Rev. B* 72, 094432 (2005).
- [10] M. Schäfers, V. Drewello, G. Reiss, A. Thomas, K. Thiel, G. Eilers, M. Münzenberg, H. Schuhmann and M. Seibt, Electric breakdown in ultrathin MgO tunnel barrier junctions for spin-transfer torque switching, *Appl. Phys. Lett.* 95, 232119 (2009).
- [11] D.V. Dimitrov, Z. Gao, X. Wang, W. Jung, X. Lou and O.G. Heinonen, Dielectric breakdown of MgO magnetic tunnel junctions, *Appl. Phys. Lett.* 94, 123110 (2009).
- [12] C. Yoshida, M. Kurasawa, Y.M. Lee, K. Tsunoda, M. Aoki and Y. Sugiyama, A study of dielectric breakdown mechanism in CoFeB/MgO/CoFeB magnetic tunnel junction, *IEEE Int. Reliab. Phys. Symp.*, 139-142 (2009).
- [13] X. Fong, Y. Kim, R. Venkatesan, S.H. Choday, A. Raghunathan and K. Roy, Spin-transfer torque memories: Devices, circuits, and systems, *Proc. IEEE* 104, 1449-1488 (2016).
- [14] S.K. Gupta, S.P. Park, N.N. Mojumder and K. Roy, Layout-aware optimization of STT MRAMs, *Proc. Design Autom. Test Eur. Conf. Exhibit.* 1455-1458 (2012).
- [15] Y. Shiota, T. Nozaki, F. Bonell, S. Murakami, T. Shinjo and Y. Suzuki, Induction of coherent magnetization switching in a few atomic layers of FeCo using voltage pulses, *Nat. Mater.* 11, 39-43 (2012).
- [16] K. Wang, J. Alzate and P.K. Amiri, Low-power non-volatile spintronic memory: STT-RAM and beyond, *J. Phys. D: Appl. Phys.* 46, 074003 (2013).
- [17] S. Yuasa, A. Fukushima, K. Yakushiji, T. Nozaki, M. Konoto, H. Maehara, H. Kubota, T. Taniguchi, H. Arai and H. Imamura, Future prospects of MRAM technologies, *IEEE Int. Electron Devices Meet.* (2013).
- [18] C. Grezes, F. Ebrahimi, J. Alzate, X. Cai, J. Katine, J. Langer, B. Ocker, P.K. Amiri and K. Wang, Ultra-low switching energy and scaling in electric-field-controlled nanoscale magnetic tunnel junctions with high resistance-area product, *Appl. Phys. Lett.* 108, 012403 (2016).
- [19] S. Kanai, M. Yamanouchi, S. Ikeda, Y. Nakatani, F. Matsukura and H. Ohno, Electric field-induced magnetization reversal in a perpendicular-anisotropy CoFeB-MgO magnetic tunnel junction, *Appl. Phys. Lett.* 101, 122403 (2012).
- [20] S. Kanai, F. Matsukura and H. Ohno, Electric-field-induced magnetization switching in CoFeB/MgO magnetic tunnel junctions with high junction resistance, *Appl. Phys. Lett.* 108, 192406 (2016).
- [21] B.W. Wilson, K. Caputa, M.A. Stuchly, J.D. Saffer, K.C. Davis, C.E. Washam, L.G. Washam, G.R. Washam and M.A. Wilson, Design and fabrication of well confined uniform magnetic field exposure systems, *Bioelectromagnetics* 15, 563-577 (1994).
- [22] M. Kreissig, R. Lebrun, F. Protze, K. Merazzo, J. Hem, L. Vila, R. Ferreira, M. Cyrille, F. Ellinger and V. Cros, Vortex spin-torque oscillator stabilized by phase locked loop using integrated circuits, *AIP Adv.* 7, 056653 (2017).

- [23] B. Lacoste, M.M. de Castro, R. Sousa, I. Prejbeanu, L. Buda-Prejbeanu, S. Auffret, U. Ebels, B. Rodmacq and B. Dieny, Control of Sub-Nanosecond Precessional Magnetic Switching in STT-MRAM Cells for SRAM Applications, IEEE Int. Memory Workshop, (2016).
- [24] S. Ikeda, K. Miura, H. Yamamoto, K. Mizunuma, H. Gan, M. Endo, S. Kanai, J. Hayakawa, F. Matsukura and H. Ohno, A perpendicular-anisotropy CoFeB–MgO magnetic tunnel junction, Nat. Mater. 9, 721-724 (2010).
- [25] R. Heindl, W. Rippard, S. Russek, M. Pufall and A. Kos, Validity of the thermal activation model for spin-transfer torque switching in magnetic tunnel junctions, J. Appl. Phys. 109, 073910 (2011).
- [26] A. Jaiswal, X. Fong and K. Roy, Comprehensive Scaling Analysis of Current Induced Switching in Magnetic Memories Based on In-Plane and Perpendicular Anisotropies, IEEE J. Emerg. Sel. Topics Circuits Syst. 6, 120-133 (2016).
- [27] J.C. Slonczewski, Current-driven excitation of magnetic multilayers, J. Magn. Magn. Mater., 1996, pp. L1-L7.
- [28] A. Timopheev, R. Sousa, M. Chshiev, L. Buda-Prejbeanu and B. Dieny, Respective influence of in-plane and out-of-plane spin-transfer torques in magnetization switching of perpendicular magnetic tunnel junctions, Phys. Rev. B 92, 104430 (2015).
- [29] G. Gupta, Z. Zhu and G. Liang, Switching based Spin Transfer Torque Oscillator with zero-bias field and large tuning-ratio, arXiv:1611.05169v2 (2016).
- [30] D. Chien, X. Li, K. Wong, M.A. Zurbuchen, S. Robbenolt, G. Yu, S. Tolbert, N. Kioussis, P. Khalili Amiri and K.L. Wang, Enhanced voltage-controlled magnetic anisotropy in magnetic tunnel junctions with an MgO/PZT/MgO tunnel barrier, Appl. Phys. Lett. 108, 112402 (2016).
- [31] W.-G. Wang, M. Li, S. Hageman and C. Chien, Electric-field-assisted switching in magnetic tunnel junctions, Nat. Mater. 11, 64-68 (2012).
- [32] X. Li, G. Yu, H. Wu, P. Ong, K. Wong, Q. Hu, F. Ebrahimi, P. Upadhyaya, M. Akyol and N. Kioussis, Thermally stable voltage-controlled perpendicular magnetic anisotropy in Mo|CoFeB| MgO structures, Appl. Phys. Lett. 107, 142403 (2015).
- [33] W. Skowroński, T. Nozaki, D.D. Lam, Y. Shiota, K. Yakushiji, H. Kubota, A. Fukushima, S. Yuasa and Y. Suzuki, Underlayer material influence on electric-field controlled perpendicular magnetic anisotropy in CoFeB/MgO magnetic tunnel junctions, Phys. Rev. B 91, 184410 (2015).
- [34] W. Skowroński, T. Nozaki, Y. Shiota, S. Tamaru, K. Yakushiji, H. Kubota, A. Fukushima, S. Yuasa and Y. Suzuki, Perpendicular magnetic anisotropy of Ir/CoFeB/MgO trilayer system tuned by electric fields, Appl. Phys. Express 8, 053003 (2015).
- [35] M. Beleggia, M. De Graef, Y. Millev, D. Goode and G. Rowlands, Demagnetization factors for elliptic cylinders, J. Phys. D: Appl. Phys. 38, 3333 (2005).
- [36] M. Beleggia, M. De Graef and Y. Millev, The equivalent ellipsoid of a magnetized body, J. Phys. D: Appl. Phys. 39, 891 (2006).
- [37] H. Sato, S. Ikeda, S. Fukami, H. Honjo, S. Ishikawa, M. Yamanouchi, K. Mizunuma, F. Matsukura and H. Ohno, Co/Pt multilayer based reference layers in magnetic tunnel junctions for nonvolatile spintronics VLSIs, Jpn. J. Appl. Phys. 53, 04EM02 (2014).
- [38] M. Franchin, Multiphysics simulations of magnetic nanostructures (Doctoral dissertation, University of Southampton, 2009).
- [39] W. Skowroński, P. Ogorodnik, J. Wrona, T. Stobiecki, R. Świrkowicz, J. Barnaś, G. Reiss and S. van Dijken, Backhopping effect in magnetic tunnel junctions: Comparison between theory and experiment, J. Appl. Phys. 114, 233905 (2013).
- [40] S. Sharma, B. Muralidharan and A. Tulapurkar, Proposal for a domain wall nano-Oscillator driven by non-uniform spin currents, arXiv:1509.01791 (2015).
- [41] W. Scholz, T. Schrefl and J. Fidler, Micromagnetic simulation of thermally activated switching in fine particles, J. Magn. Magn. Mater. 233, 296-304 (2001).
- [42] M.J. Werner and P.D. Drummond, Robust Algorithms for Solving Stochastic Partial Differential Equations, J. Comput. Phys. 132, 312-326 (1997).
- [43] D. Berkov and N. Gorn, Numerical simulation of quasistatic and dynamic remagnetization processes with special applications to thin films and nanoparticles, Handb. Adv. Magn. Mater. 794-880 (2006).
- [44] H. Akimoto, H. Kanai, Y. Uehara, T. Ishizuka and S. Kameyama, Analysis of thermal magnetic noise in spin-valve GMR heads by using micromagnetic simulation, J. Appl. Phys. 97, 10N705 (2005).
- [45] A. Vansteenkiste, J. Leliaert, M. Dvornik, M. Helsen, F. Garcia-Sanchez and B. Van Waeyenberge, The design and verification of MuMax3, AIP Adv. 4, 107133 (2014).
- [46] H. Kubota, A. Fukushima, K. Yakushiji, T. Nagahama, S. Yuasa, K. Ando, H. Maehara, Y. Nagamine, K. Tsunekawa, D.D. Djayaprawira, N. Watanabe and Y. Suzuki, Quantitative measurement of voltage dependence of spin-transfer torque in MgO-based magnetic tunnel junctions, Nat. Phys. 4, 37-41 (2008).

- [47] K. Bernert, Spin-transfer torques in MgO-based magnetic tunnel junctions (Doctoral Thesis, Technische Universität Dresden, 2014).
- [48] Z. Kugler, V. Drewello, M. Schäfers, J. Schmalhorst, G. Reiss and A. Thomas, Temperature and bias voltage dependence of Co/Pd multilayer-based magnetic tunnel junctions with perpendicular magnetic anisotropy, *J. Magn. Magn. Mater.* 323, 198-201 (2011).
- [49] J.C. Sankey, Y.-T. Cui, J.Z. Sun, J.C. Slonczewski, R.A. Buhrman and D.C. Ralph, Measurement of the spin-transfer-torque vector in magnetic tunnel junctions, *Nat. Phys.* 4, 67-71 (2008).
- [50] X. Waintal, E.B. Myers, P.W. Brouwer and D. Ralph, Role of spin-dependent interface scattering in generating current-induced torques in magnetic multilayers, *Phys. Rev. B* 62, 12317 (2000).
- [51] S. Hernández and R. Victora, Calculation of spin transfer torque in partially polarized spin valves including multiple reflections, *Appl. Phys. Lett.* 97, 062506 (2010).
- [52] W. Zhu, Z. Zhang, J. Zhang and Y. Liu, Multiple Reflection Effect on Spin-Transfer Torque Dynamics in Spin Valves with a Single or Dual Polarizer, *Spin*, World Scientific, 5, 1550003 (2015).
- [53] R. Bell, J. Hu and R.H. Victora, Dual Referenced Composite Free Layer Design for Improved Switching Efficiency of Spin-Transfer Torque Random Access Memory, *IEEE Electron Device Lett.* 37, 1108-1111 (2016).
- [54] J. Slonczewski, Currents, torques, and polarization factors in magnetic tunnel junctions, *Phys. Rev. B* 71, 024411 (2005).
- [55] M. Julliere, Tunneling between ferromagnetic films, *Phys. Lett. A* 54, 225-226 (1975).
- [56] S. Mangin, D. Ravelosona, J. Katine, M. Carey, B. Terris and E.E. Fullerton, Current-induced magnetization reversal in nanopillars with perpendicular anisotropy, *Nat. Mater.* 5, 210-215 (2006).
- [57] N. Hiroki, I. Kazutaka, A. Keiko, F. Shinobu, S. Yoichi, N. Takayuki, Y. Shinji and S. Yoshishige, Novel Voltage Controlled MRAM (VCM) with Fast read write circuits for ultra large last level cache, *IEEE Int. Electron Devices Meet.* (2016).
- [58] Y. Shiota, T. Nozaki, S. Tamaru, K. Yakushiji, H. Kubota, A. Fukushima, S. Yuasa and Y. Suzuki, Evaluation of write error rate for voltage-driven dynamic magnetization switching in magnetic tunnel junctions with perpendicular magnetization, *Appl. Phys. Express* 9, 013001 (2015).
- [59] G. Han, H. Meng, J. Huang, V.B. Naik, C.H. Sim, M. Tran and S. Ter Lim, Perspectives of Electric Field Controlled Switching in Perpendicular Magnetic Random Access, *IEEE Trans. Magn.* 51, 1-9 (2015).
- [60] J. Kalisz, A. Poniecki and K. Rózyk, A simple, precise, and low jitter delay/gate generator, *Rev. Sci. Instrum.* 74, 3507-3509 (2003).
- [61] E. Cetin and T. Kuyel, Hundred femtosecond jitter measurement using dual-channel ADC with imprecise clock stimulus, *Electron. Lett.* 48, 1525-1526 (2012).
- [62] R.F. Freitas and W.W. Wilcke, Storage-class memory: The next storage system technology, *IBM J. Res. Dev.* 52, 439-447 (2008).
- [63] C.H. Lam, Storage class memory, *Proc. IEEE Solid-State and Integrated Circuit Technology*, 1080-1083 (2010).
- [64] M. Moshayedi and P. Wilkison, Enterprise ssds, *Queue* 6, 32-39 (2008).
- [65] R.-S. Liu, C.-L. Yang and W. Wu, Optimizing NAND flash-based SSDs via retention relaxation, *Target* 11, 00 (2012).
- [66] D. Kyriazis, Data Intensive Storage Services for Cloud Environments, IGI Global, (2013).
- [67] C.W. Smullen, V. Mohan, A. Nigam, S. Gurumurthi and M.R. Stan, Relaxing non-volatility for fast and energy-efficient STT-RAM caches, *IEEE Int. Symp. High Performance Computer Architecture*, 50-61 (2011).
- [68] D. Saida, S. Kashiwada, M. Yakabe, T. Daibou, N. Hase, M. Fukumoto, S. Miwa, Y. Suzuki, H. Noguchi and S. Fujita, Sub-3 ns pulse with sub-100 μ A switching of 1x-2x nm perpendicular MTJ for high-performance embedded STT-MRAM towards sub-20 nm CMOS, *IEEE Symp. VLSI Technol.* (2016).
- [69] K. Wang and P.K. Amiri, Nonvolatile spintronics: perspectives on instant-on nonvolatile nanoelectronic systems, *Spin*, World Scientific, 2, 1250009 (2012).
- [70] J. Mazierska, D. Ledenyov, M.V. Jacob and J. Krupka, Precise microwave characterization of MgO substrates for HTS circuits with superconducting post dielectric resonator, *Supercon. Sci. Technol.* 18, 18 (2004).
- [71] S. Ingvarsson, M. Arikan, M. Carter, W. Shen and G. Xiao, Impedance spectroscopy of micron sized magnetic tunnel junctions with MgO tunnel barrier, *Appl. Phys. Lett.* 96, 232506 (2010).

Figures

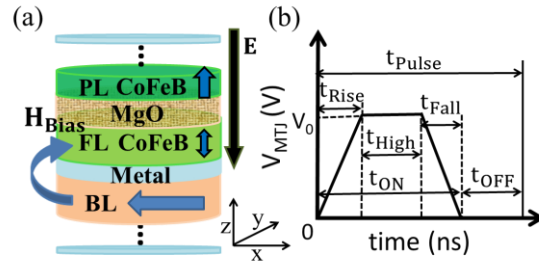


Figure 1. (a) Schematic of an elliptical pMTJ with the major axis along the x-axis. A bias layer (BL) separated by a metal is engineered to provide the exchange field for the FL. The top and bottom water-blue layers are electrodes. (b) The applied voltage pulse with $t_{Rise} = t_{Fall} = 50$ ps and t_{OFF} of 10 ns, which is long enough to ensure that the magnetization is completely relaxed. Positive voltage is defined for the electric field pointing from the PL to the FL.

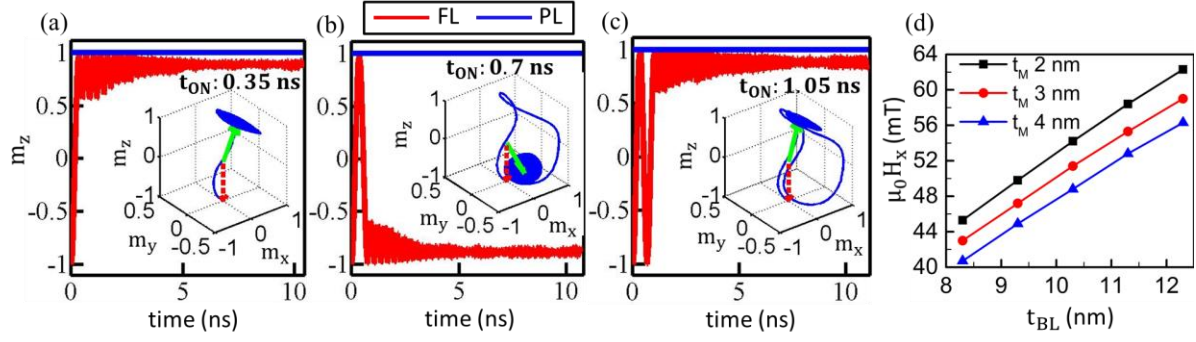


Figure 2. FL switching for a voltage pulse with t_{ON} in integer multiples of the half precession periods (t_{Half}): t_{ON} is (a) 0.35 ns, (b) 0.7 ns and (c) 1.05 ns while t_{Half} is 0.35 ns. For the odd multiples the FL toggles while for the even cases it restores to the original state and remains unaltered. Insets show a full three dimensional (3D) FL dynamics for the respective cases, where the red dash arrow, green arrow and blue line is the initial \mathbf{m} state, final \mathbf{m} state and its trajectory, respectively. (d) The exchange field acting on the FL along the x-axis generated by the BL for different metal spacer thicknesses t_M and BL thicknesses t_{BL} . This large enough exchange field, e.g. 50 mT for the t_{BL} of 10 nm and the t_M of 3 nm, can bias the FL for the precession based VCMA switching.

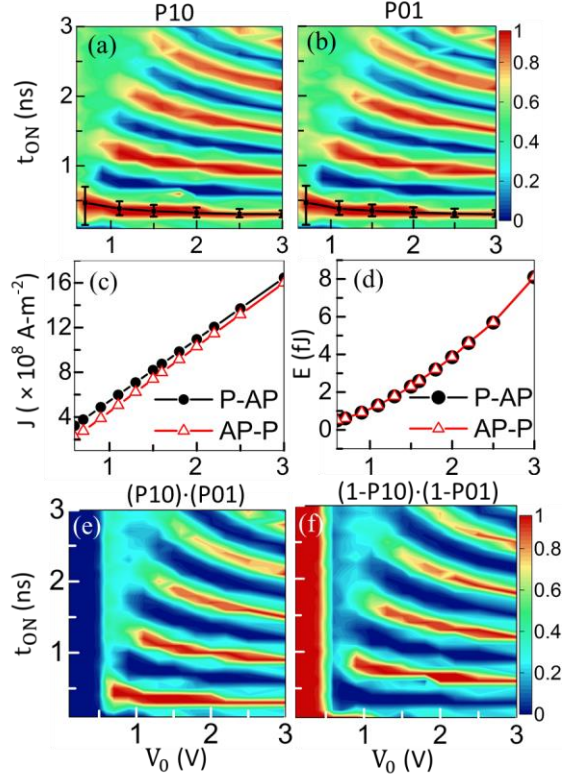


Figure 3. Phase diagram for switching probability from (a) parallel (P) to anti-parallel (AP) state (P10) and from (b) AP-to-P (P01) as a function of t_{ON} and V_0 for a t_{MgO} of 2 nm and a bias field $\mu_0 H_x$ of 50 mT (with thermal fluctuation). The black bars show the t_{ON} operation windows without considering the thermal fluctuation. The increasing operation window as the V_0 decreases indicates that the device favors a low-voltage operation. (c) Current density and (d) energy consumption per switch *vs.* V_0 . (e) Switching probability from P-to-AP ‘AND’ AP-to-P (P10·P01) as a function of t_{ON} and V_0 . Red regions indicate deterministic switching, i.e. 100% certainty of toggling. (f) Retention probability, i.e. $(1-P10) \cdot (1-P01)$ as a function of t_{ON} and V_0 . Red regions show with 100% probability that pre-configured data would not be altered.

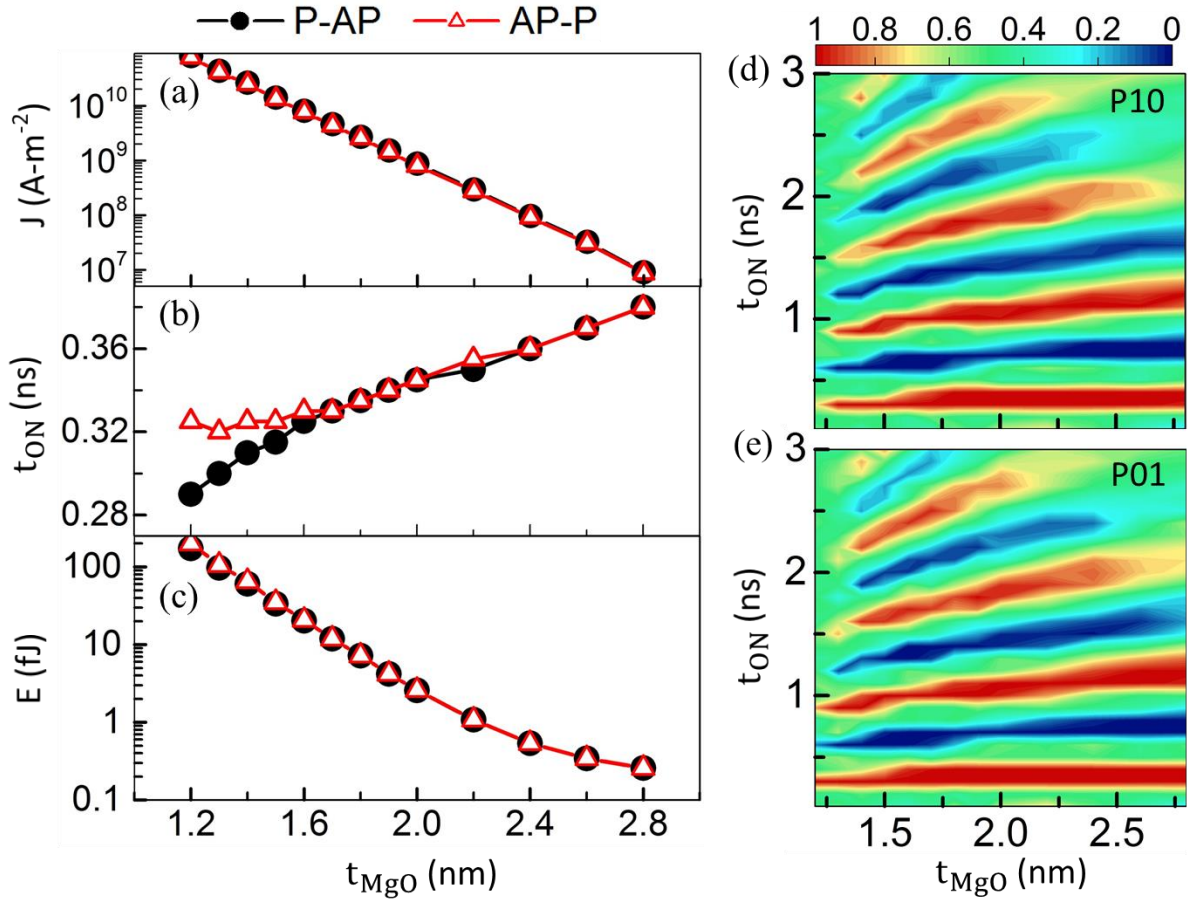


Figure 4. Effects of t_{MgO} on (a) current density, (b) t_{ON} (optimal values used to switch, i.e. t_{Half}) and (c) energy consumption per switching operation at 1.6 V V_0 and 50 mT $\mu_0 H_x$. Red lines with open triangles show the process from AP-to-P. Black lines with solid circles correspond to the process from P-to-AP. The smallest switching energy achieved is 0.3 fJ. Phase diagram for switching probability from (d) P-to-AP and (e) AP-to-P vs. t_{ON} and t_{MgO} .

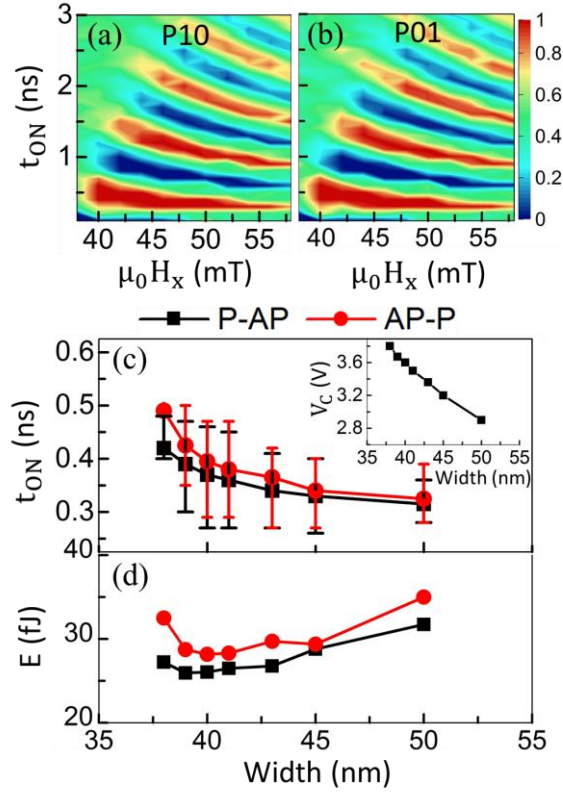


Figure 5. Phase diagram for switching probability of (a) P-to-AP and (b) AP-to-P as a function of t_{ON} and bias magnetic field $\mu_0 H_x$. H_x is the magnitude of \mathbf{H}_{Bias} projecting along x-axis. Optimal t_{ON} used to switch (t_{Half}) in (c) and energy consumption in (d) as a function of the MTJ width. The AR and FL thickness are held constant at 3 and 1.7 nm respectively, e.g. for width of 40 nm, the MTJ cross-section is $40 \times 120 \text{ nm}^2$. The inset shows the critical voltage V_C vs. the MTJ width.